Research Article

Dominant Oscillations and Long-Term Trends Observed in the Stratosphere and Lower Mesosphere Using Rayleigh Lidar

[1]Vennapu Lakshmana Rao, [2] P. Srinivasa Rao

[1]Assistant Professor (c), Dept. of Meteorology and Oceanography, Andhra University, Visakhapatnam, India
[2]Researches Scholar, Dept. Of Meteorology and Oceanography, Andhra University, Visakhapatnam, India

ABSTRACT

The aim of this study describes the Rayleigh system and data acquisition that were used to retrieve the temperature in detail. In the present study the long term data are available from Lidar system, which is located at Gadanki (13.5°N, 79.2°E). In this article we have investigated the long term variations such as Annual, Semi-annual, Quasi- biennial, Elnino Southern Oscillation and the solar cycle. In the present study an attempt is made the use long term temperature data from the Gadanki Lidar located at a low latitude station, long- term trends observed in the temperatures are reported. Here we have taken temperature data for observing mean temperature inversions from the period of 1998- 2010. The phases of the SAO and AO observed by the Lidar show a downward progression below 60 km, and above that altitude no clear phase progression is seen. The thermal structure also observed using Gadanki Lidar. The Lidar data during night time in the monsoon season (June - October) are considerably less than those other seasons. The clear temperature variations in peak temperature lying in the range of 264 – 266K during February – April and September – October around 70 – 80 Km is showing clear semiannual oscillation. These semiannual oscillations correspond to the Stratopause semiannual oscillation and Mesospheric Semiannual Oscillation (MSAO). In this article monthly occurrence of Mesospheric temperature inversions also consider with me. The peak occurrence is seen during March and October, broad maximum from March _ May and September _ November can be noticed.

Keywords: SAO, Semi-annual, Quasi- biennial, Elnino Southern Oscillations, Solar cycle, Ionosphere, Mesosphere, Energetic and Dynamics.

1. INTRODUCTION

Many different techniques are currently used to study the atmosphere, including radars, lidars, satellites and rockets, each with its own advantages and disadvantages. Ground based remote sensing techniques such as radars and lidars have advantages of continuous measurements with good time and height resolution. Even though, the rocket observations have high resolution, the accuracy is poor compared to radar and lidar. The data used for present study was obtained from ground based Rayleigh lidar system located Gadanki (13.5°N, 79.2°E). This study describes the Rayleigh system and data acquisition that were used to retrieve the temperature in detail.

In recent days, climate change is posing unprecedented serious challenges that society has ever faced. There is now an overwhelming consensus that human activities have been affecting the composition of Earth's atmosphere. The scientific facts are clear – recognized by the Nobel Prize in 2007 - that phase of climate change is accelerating and it is endangering our safety and economic development. Its fingerprints are felt on our planet's glaciers to its ocean depths, from its lush plains to its arid steppes. Over the last three to four decades, significant progress has been made in observing, understanding and to some extent predicting the variability and changes in Earth's climate system. Impressive progress in climate science, reflected notably in the recent assessment report of the

---

Corresponding Author: Vennapu Lakshmana Rao
Email: lakshman.met@gmail.com

Intergovernmental Panel on Climate Change (IPCC 2007) provided robust findings on the cause of climate change and its impacts over the next decades. It was realized recently that the perturbations in atmospheric parameters caused by various human activities are not only confined to the lower atmosphere, but also most likely extends into middle and upper atmosphere [Beig et al., 2003]. In view of this, it has become more important and vital to study the variations due to natural activities in parameters affecting climate and to distinguish them from perturbations induced by global change. As the amplitudes increase with respect to altitude due to decreasing densities, it is also believed that pronounced effects of climate change will be noticed at higher altitudes. Here, we concentrate on the affects of climate change in the tropical middle atmosphere. In recent global-mean cooling of the stratosphere is widely viewed as evidence for a discernible anthropogenic impact on the climate system. This assessment is based on the longest temperature data set (~17 years) having a global coverage of radiance measurements performed by the successive NOAA satellites since 1979. Temperature trends derived from radiosonde data show a stronger cooling trend as compared to satellite measurements [Seidel et al., 2001; Lanzante et al., 2003a, b; Randel and Wu, 2006]. Temperature variability associated with the 11-year solar cycle, El Nino-Southern Oscillation (ENSO), and the Quasi-Biennial Oscillation (QBO) has been found to be prominent in the lower and middle atmosphere, and plays a key role in the overall balance of its composition and circulation [Reid, 1994]. The QBO is one of several possible "external" influences on the inter-annual variability of the northern stratospheric flow. Other possible, forcing includes the solar cycle (with effects probably strongest in the equatorial upper stratosphere associated with ozone heating), the remote effects of ENSO, and forcing from below by tropospheric circulation anomalies [Baldwin and O'sullivan, 1994]. Recently Li et al. [2008] reported inter-annual variability associated with the 11-year solar cycle, ENSO, and the QBO using Hawaii Lidar temperature from 1994 to 2007 between 15 and 85 km. They revealed the dominance of the QBO (1-3 K) in the stratosphere and mesosphere, stronger winter signatures of ENSO in the troposphere and lower stratosphere (~1.5 K/MEI),

and maxima of solar cycle ~1.3 K/100 F10.7 units at 35 and 55 km. A number of studies [Sridharan et al., 2009; Keckhut et al., 2005; Remsberg and Deaver, 2005; Fadnavis and Beig, 2006; Clemesha et al., 1997] on 11-year solar cycle using the temperature data set also exist.

Recent observations and global circulation models predict that the increasing emissions of greenhouse gases have a profound effect on the thermal structure of the middle atmosphere [Beig et al., 2003]. To understand the dynamics of the middle atmosphere, which can be modulated by the waves such as gravity and planetary waves, the basic thermal structure is one of the primary sources. It is also important to understand the radioactive and chemical processes and coupling between different regions of the atmosphere.

The advancement in satellite remote sensing has offered a variety of satellites for global temperature observations. Space-borne instruments like Pressure Modulated Radiometer (PMR), Improved Stratospheric and Mesospheric Sounder (ISAMS), Solar Mesosphere Explorer (SME), Limb Infrared Monitor of the Stratosphere (LIMS), Selective Shopper Radiometer (SCR), Halogen Occultation Experiment (HALOE) and WIND Imaging Interferometer (WINDII) have been used to study the thermal structure of the middle atmosphere. However their revisit times are limited over the selected locations. LIMS provided only two observations (1300 LT and 2300 LT) at the equator per day during 1978-79 [Gille and Russell, 1984; Remsberg el al. 2004]. HALOE measured temperature in the altitude region of 20-90 km during sunrise and sunset only [Leblanc and Hanchecorne, 1997; Wit el al, 2003].

2. DATA AND METHODOLOGY

The below figure 1 shows the location of the Gadanki. Details of this technique are presented below.
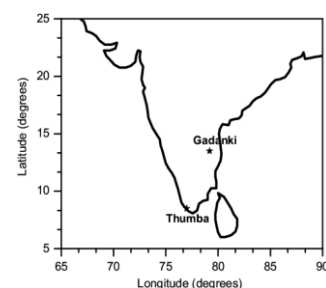

Fig.1: Study Area Map

Map shows the location of Gadanki where the Rayleigh Lidar system is located.

2.1 Gadanki Rayleigh lidar

Lidar, based on the same principle of radar, offers a powerful technique to probe the atmospheric structure and dynamics with high spatial and temporal resolutions. The state-of-the-art Rayleigh Lidar is co-located in the Indian MST radar. It provides information of temperature (density) in height range of 30-80 km with a high range resolution of 300 m. **Figure 2** shows the block diagram of the Rayleigh lidar and its picture taken during one of the nights operation is depicted in **Figure 3.**
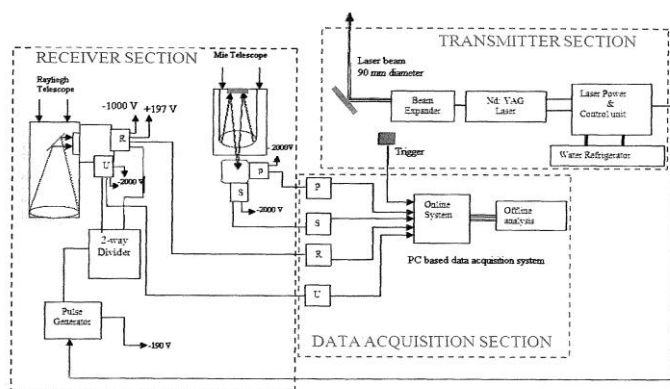

Fig.2: Functional block diagram of Rayleigh lidar located at Gadanki.

Rayleigh Lidar employs an Nd: YAG pulsed laser which is a solid state class of laser sources. It uses the second harmonic output of the laser source at 532 nm with a maximum energy of 550 mJ per pulse. It operates a with pulse repetition frequency of 20 Hz and a pulse width of 7 ns. The laser optical properties are specified as 0.45 m rad for divergence and 1 cm^{-1} for line-width and 9 mm in beam size. The laser control system consists of high-tension (HT) supplies and capacitor banks for an amplifier and oscillator assemblies of laser sources, interlock electronics and a distilled water pump for cooling the amplifier and oscillator head assemblies.

The laser beam is made to pass through a beam expander (expand 10 times), before allowing to send into the sky. Hence, the transmit beam divergence is reduced from 0.45m rad to less than 0.1m rad. The expanded beam of 90 mm width is made to fall on a steering mirror, which is a hard coated flat type mirror with the dimensions of 154 mm diameter and 25 mm thickness oriented at 45° to the beam axis. The mirror is provided with azimuth and elevation controls to align the transmit beam axis

to receive beam axis. The major specifications of the system are summarized in the

Table 1: Major Specifications of Gadanki Rayleigh lidar

Parameter	Specifications
Laser source	Nd:YAG
Operating Wavelength	532 nm
Average energy for pulse	550 mJ
Average output power	11 W
Pulse width	7 nsec
Pulse repetition frequency	20 Hz
Beam width	9 mm (Expanded to 90 mm)
Beam divergence	0.1 m rad
Telescope type	Newtonian
Diameter	750mm
Field of view	1 m rad
Interference filter bandwidth	1.07nm
Maximum transmission	48%
Bin width	2 U.S6C
Scan length	1024 channel
Integration time	250 sec (corresponds to 5000 laser shots)
Range resolution	300m

The receiver subsystem employs two independent receivers to receive Rayleigh and Mie backscattered signals from the atmosphere. The Rayleigh receiver is used for collecting the backscattered light from the air molecules and operates in the range of 30 to 80 km, whereas the Mie receiver is used for collecting the backscattered light from the particles such as aerosols, hydrometeors, clouds etc., in the range of 7 to 30 km. The Rayleigh receiver employs to a Newtonian telescope with a primary mirror having an effective diameter of 75 cm with a focal length of 2372 mm for molecular density/ temperature measurements over the altitude region of-30-80 km.

The secondary mirror is a plane mirror of diameter of 250 mm oriented at 45° to the receiver optics beam axis facing primary mirror. The secondary mirror focuses the beam at field stop iris, which, in turn, falls on a collimating lens. The collimating lens directs the beam to an interference filter, with Full Width Half Maximum of 1.07 nm which rejects much of the background light and passes only the monochromatic spectrum at 532 nm wavelength. This band-limited light is made to fall on a non-polarizing beam splitter. This beam splitter splits the beam into two equal halves and made to fall on the cathode surface of head-on type of photomultiplier tubes (PMTs) aligned along the beam axis and fixed to the beam splitter assembly. The signal is then split into two channels in the ratio of 9:1; the high gain

channel (R) covers 50-80 km where the signal is weak and the low gain channel (U) covers 30-50 km where the signal is relatively stronger. The signals are directed to PMTs. Both the PMTs work at a HT potential of −2 kV. These PMTs are kept in the magnetic shield enclosure to avoid the exposure to external fields. The PMTs are delayed or gated by duration of 80 μs, this is achieved by applying a positive pulse of +197 V. It is being done to prevent the loading of PMTs from the large amount of back-scattered photons that arises from the lower atmosphere. The outputs drive-Philips makes pulse discriminators which contain 300 MHz pulse amplifier with a threshold adjustable compactor and a shaper circuit. These discriminators operate with no dead time for coincidence applications. It has a 15-turn potentiometer adjustment for a threshold that provides a pulse width increment from 2 ns to 50 ns for corresponding threshold adjustments from -1 mV to -100 mV. It has a veto input, which accepts a Network Interface Machine (NIM) standard level pulse that inhibits the function of the discriminator. The output of the discriminator is a current source type, which drives long cables with narrow pulse widths at −32 mA. The output of pulse discriminators is connected to a PC based photon counting data acquisition system operating under an EG and G Multi Channel Software (MCS).

2.2 Temperature retrieval

The method of analysis adopted for the determination of temperature profile closely follows that given by Hauchecorne and Chanin [1980]. In the height range 30-80 km, where Mie contribution is negligible, the range and atmospheric transmission corrected signal intensity is proportional to the molecular number density. Using the number density taken from an appropriate model [CIRA-1976] for the height of 50 km where the signal-to-noise ratio is fairly high, the constant of proportionality is evaluated and there by the density profile is derived. Taking the pressure at the top of the height range (90 km) from an atmospheric model, the pressure profile is computed using the measured density profile, assuming the atmosphere to be in hydrostatic equilibrium. The model atmosphere used for the purpose is CIRA-86. Adopting the

perfect gas law, the temperature profile is computed using the derived density and pressure profiles.

$$\rho(z) = \frac{C[S_L(z) - B(z)]}{t^2(z,\alpha)} \qquad \dots 2.1$$

Where $S_L(z)$ is the range corrected signal intensity, B(z) is the signal due to dark current and sky background, t(z, α) is the atmospheric transmittance between z and the top of the atmosphere and C is the normalization constant.

The air pressure P (z), density ρ(z) and temperature T (z) are related by

$$\rho(z) = \frac{RT(z)\rho(z)}{M} \qquad \dots 2.2$$

Where 'p (z)' density at an altitude z and M is the mean molecular weight of air.

According to the hydrostatic equilibrium, the acceleration due to gravity in terms of density and pressure gradient is given by

$$g(z) = \left(\frac{-1}{\rho(z)}\right)\frac{dP}{dz} \qquad \dots 2.3$$

(or)   dP(z) - −ρ(z)g(z)dz 2.4

Hence $\dfrac{dP}{P} = \left(\dfrac{Mg(z)dz}{RT(z)}\right) \qquad \dots 2.5$

But $d[\log(P(z))] = \dfrac{dP(z)}{P(z)}$, Hence Eq. 2.15 becomes

$$d[\log(P(z))] = -\left(\frac{Mg(z)dz}{RT(z)}\right) \qquad \dots 2.6$$

$$\frac{P\left(z - \dfrac{dz}{2}\right)}{P\left(z + \dfrac{dz}{2}\right)} = \exp\left(\frac{Mg(z)dz}{RT(z)}\right) \text{ (or)}$$

$$\log\left(\frac{P\left(z - \dfrac{dz}{2}\right)}{P\left(z + \dfrac{dz}{2}\right)}\right) = \left(\frac{Mg(z)dz}{RT(z)}\right) \qquad \dots 2.7$$

$$T(z) = \left(\frac{Mg(z)dz}{R\log(1+X)}\right) \text{ Where } X = \frac{\rho(z)g(z)dz}{P\left(z + \dfrac{dz}{2}\right)} \qquad \dots 2.8$$

The temperature profile can be obtained using the above Eq. 2.8 and the uncertainty in temperature is found to be 15% at 90 km where the pressure is assumed. The pressure contribution

to the temperature uncertainty decreases rapidly with altitude and it seems to be smaller than 2% at 15 km below the top.

i.e., $\dfrac{\delta T(z)}{T(z)} = \dfrac{\delta[\log(1+X)]}{\log(1+X)} = \dfrac{\delta X}{(1+X)\log(1+X)}$ ... 2.9

With $\left(\dfrac{\delta X}{X}\right)^2 = \left|\dfrac{\delta\rho(z)}{\rho(z)}\right|^2 = \left|\dfrac{\delta P\left(z+\dfrac{dz}{2}\right)}{P\left(z+\dfrac{dz}{2}\right)}\right|^2$ 2.10

Initially, the atmospheric temperatures are independently computed using the relative densities derived from R and U channels. Then the composite temperature profile is constructed using data from low sensitive channel (U) for the altitude below 45 km, the high sensitive channel (R) above 55 km, and utilizing both channel's data (R and U) between 45-55 km. This region of 45-55 km employs the numerical weight function with convex convergence technique. When two simultaneous measurements are made, to converge the results and reduce the error in measurement, convex convergence technique is used [James and James, 1968]. Using the weighting factors, the temperature and standard error for the transition region are expressed as:

$T_{(45-55)}(z) = \dfrac{[T_R(z)*\delta T_U(z)]+[T_U(z)*\delta T_R(z)]}{[\delta T_R(z)+\delta T_U(z)]}$ 2.11

$\delta T_{(45-55)}(z) = \dfrac{[T_R(z)*\delta T_U(z)]+[T_U(z)*\delta T_R(z)]}{[T_R(z)+T_U(z)]}$ 2.12

Where $T_{(45-55)}$ (z) and $\delta T_{(45-55)}$ (z) stand for the temperature and the standard error for the height region of 45 to 55 km, $T_R(z)$ and $\delta T_R(z)$ are the temperature and standard error derived from R channel and $T_U(z)$ and $\delta T_U(z)$ are correspondingly for the U channel.

2.3 Statistics on the Data Available from Gadanki Rayleigh Lidar

Gadanki Rayleigh lidar was installed during early of 1998 and started giving observations since March 1998. Initially it was operated for fixed number nights in a month and the data is open to all users. It is also operated on campaign basis as and when required. Later it was realized that most number of nights its operations is required and started to operate on all clearly sky night.

3. RESULTS AND DISCUSSIONS

The below figure shows the number of the nights the Gadanki Lidar was operated in each year together with the number of nights with less than 2 hours, grater than 6 hours and between 2 and 6 hours of its operation. Out of 1498 nights of its operation, there were 212 nights, 464 nights, and 814 nights with the data available for less than 2 hours, greater than 6 hours and between 2 and 6 hours, respectively. In the initial days, there were about 80-100 nights of operation which increased to almost double since 2004.
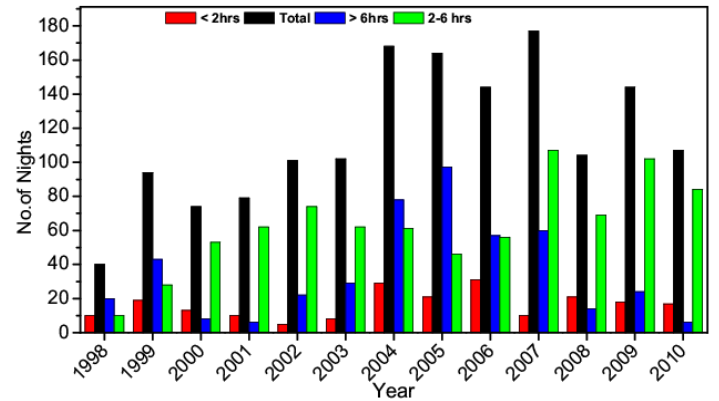

Fig.3: Years versus Number of hours

Histograms showing the total number of nights Gadanki Rayleigh Lidar were operated during 1998 to 2010. The number of nights in which lidar was operated with less than 2 hours, grater than 2 hours and in between 2 and 6 hours are also superimposed.

The above mentioned data is very much useful to investigate several issues related to temperature structure and dynamics as the data is available with a resolution of 4 minutes and 300 m vertical resolution. The data available for more than 6 hours is useful to investigate the gravity and planetary waves and their long-term trends. The data available for a minimum of 2 hours is used to investigate the long-term tends in the dominant oscillations including the long-term trends in the temperature itself. Thus, the data is further segregated for each month to know which data is useful for the gravity wave analysis and long-term trends.

The below figure shows the number of nights in which Gadanki Rayleigh Lidar data is available for different number of hours during 1998 to 2011. In general, number of nights with 2-6 hours is more irrespective of the month. The number of nights with the lidar data more than 6 hours is mostly seen during

217

winter months and very less during monsoon season. In general, this data can be used to investigate several issues.
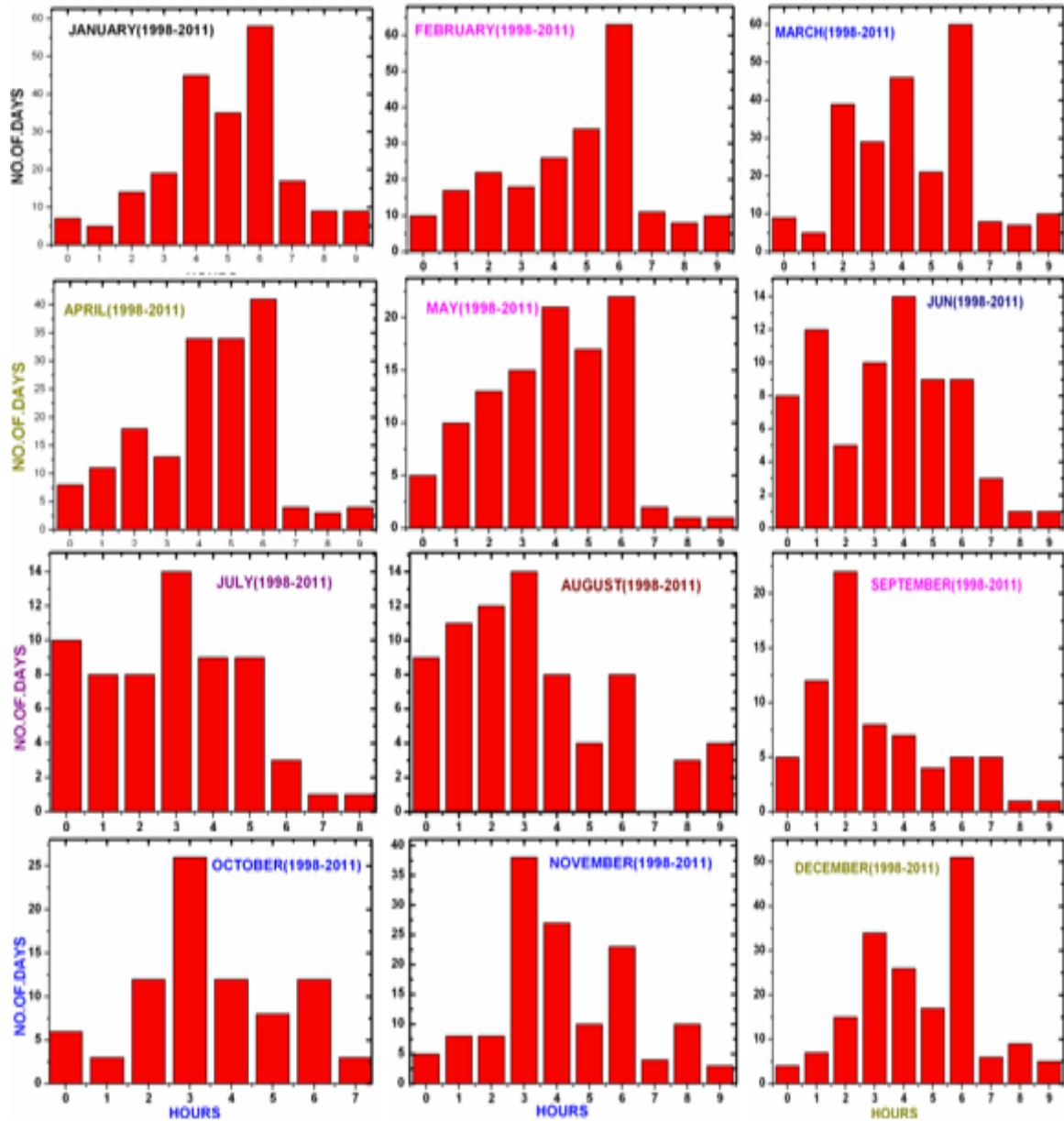

Fig.4: Histograms showing the number of nights in which Gadanki Rayleigh Lidar data is available for different number of hours during 1998 to 2011.

2.4 Thermal Structure Observed Using Gadanki Rayleigh Lidar

Figure 5 show the composite monthly mean temperature over the altitude region of 30–80 km   derived from Gadanki Lidar. Number of nights of data used in each month from this lidar is already depicted in **Figures 5** Note that in **Figure** 6 the Lidar data during nighttime in monsoon season (June–October) are considerably less than those in other seasons. **Figure 7** reveals clear temperature varied with a peak temperatures laying in the range of 264–266 K during February–April and September–

October around stratopause heights (~40–50 km) and low temperatures during March–April and September–October around 70–80 km showing clear semiannual oscillation. These semiannual oscillations correspond to the stratopause semiannual oscillation [Nee et al., 2002] and mesospheric semiannual oscillation (MSAO). These results are quite different with that observed at mid and high latitudes showing the annual oscillation, with maximum during April-July [Gobbi et al., 1995].
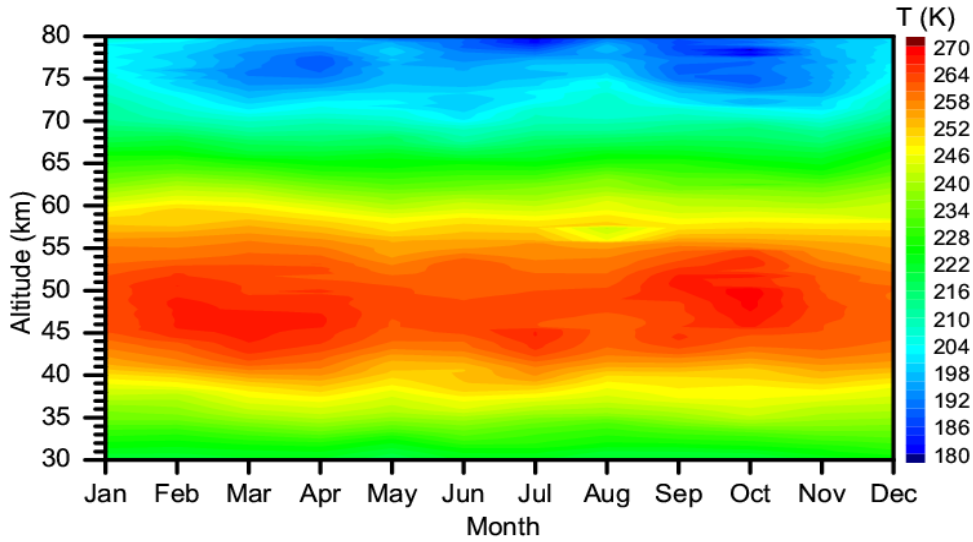
Fig.6: Composite monthly mean temperatures observed by Gadanki Rayleigh lidar during 1998–2010.

2.5 Stratopause Altitude and Temperature

The maximum temperature observed in the nightly mean profile (minimum of 2 hours of operation) is used to identify the stratopause temperature and its corresponding altitude is designated as stratopause altitude. **Figures** show the frequency distribution of the stratopause altitude and temperature obtained using the Gadanki lidar observations during 1998-2010. The frequency distribution of stratopause altitude shows wide range from 42 to 55 km with a peak around 45-47 km. The

frequency distribution of the stratopause temperature is 255-275 K with peak around 268 K. These features are found to be in good agreement with lidar observations (mean stratopause altitude of 47-48 km and mean temperature of 262 K) over Gadanki as reported by Nee et al. [2002] and Sivakumar et al. [2003] and with rocket observations (mean height of ~48 km and mean temperature of ~264 K) over Thumba as reported by Mohankumar et al. [1994].
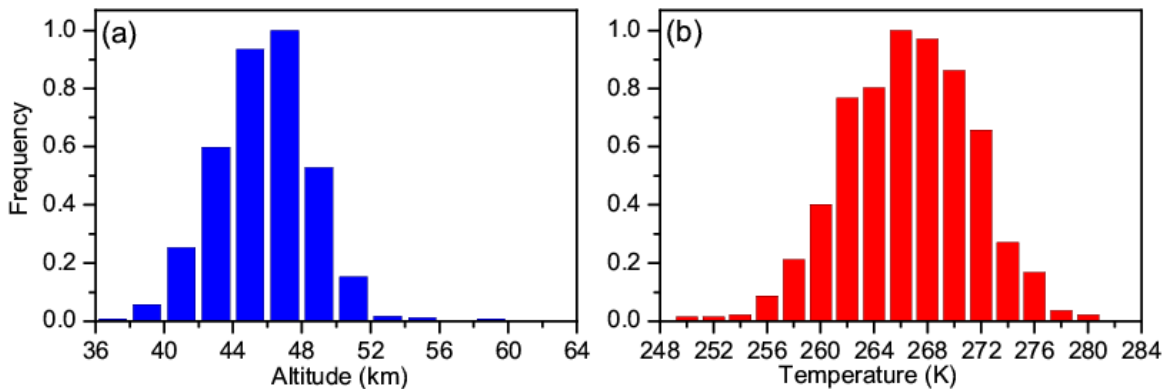

Fig.7: Frequency distribution of (a) stratopause altitude and (b) stratopause temperatures observed from Gadanki lidar observations during 1998 to 2010.

2.6 Mesospheric Temperature Inversions (MTIs) over Gadanki

As mentioned above, another aspect which is often noticed in the temperature profile over tropical mesosphere is the existence of MTIs. Using Rayleigh Lidar located at Gadanki extensive studies have been made on the possible occurrence of these MTIs. **Figure 9** shows monthly occurrence of MTIs observed during 1998-2010 using Lidar observations from Gadanki. An MTI is said to occur when the temperature increase

is more than the standard deviation for a particular height in that night. A least-square fitting for annual and semiannual variation suggest strong semiannual variation in the occurrence of MTIs with peak during equinoctial months at this station. Although the peak occurrence is seen during March and October, broad maximum from March-May and September-November can be noticed.
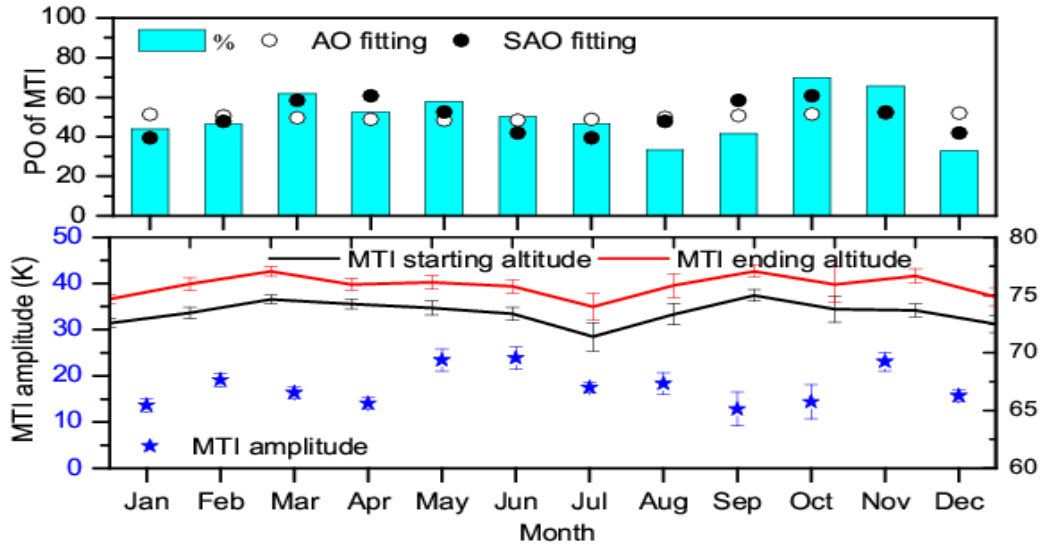
Fig.8: Months versus MTI Amplitude

(Top panel) Monthly mean percentage occurrence of mesospheric temperature inversions (MTIs) observed over Gadanki during 1998-2010. Least-squares fit for both AO and SAO is also plotted. (Bottom panel) Monthly mean variation of MTI amplitudes (left axis) and it's starting and ending heights (right axis).

The amplitude of MTIs (defined as amplitude starting from standard deviation for that night to the peak enhancement), plotted in the above figure, suggests that strong amplitudes occur during May-June and November with sharp changes in April-May and October-November months. Note that starting and ending altitude of MTIs plotted in the same panel also show maxima during the equinoxes.

2.7 Long-period Oscillations

The nightly mean temperature profiles from the lidar are averaged over a month during 1998 to 2010. Any missing data is filled with linear interpolation. Data is interpolated vertically to the uniform resolution of 1 km. Later quality checks are applied to check the consistency and continuity of the data. In general, the time-series of temperature profiles are dominated by natural periodic signals. The monthly mean temperature data is used for extracting components of semi-annul oscillations (SAO), annual oscillations (AO), quasi-biannual oscillations (QBO), ElNiño–Southern Oscillation (ENSO) and solar cycle. For extracting these oscillations one has to remove the effects of natural periodic signals mentioned above. We have applied

regression analysis to the time series at each altitude, which can be expressed as [Randel and Cobb, 1994; Randel and Wu, 2007].

$$T(t,z) = \alpha(z) + \beta(z)t + \gamma(z)QBO(t) + \delta(z)Solar(t) + \varepsilon(z)ENSO(t) + resid(t) \tag{3.1}$$

The coefficients, α, β, γ, δ, and ε are determined in a least square sense at each altitude (z) using the following expressions.

$$\alpha(z) = A_0 + \sum_{i=1}^{3}[A_i \times \cos\omega_i t + A_{i+1} \times \sin\omega_i t] \tag{3.2}$$

Where $\omega_i = 2\pi i/12$

As a QBO proxy (QBO (t)), we use Singapore monthly-mean QBO zonal winds (m/s) at 30 hPa. We used the F10.7 indices a solar proxy (solar (t)). These are Ottawa monthly-mean F10.7 solar radio flux. As an ENSO proxy ENSO (t), we use the Southern Oscillation Index (SOI), which is Tahiti (18°S, 150°W) minus Darwin (13°S, 131°E) monthly mean sea-level pressures. The long-term time series of the QBO zonal winds, F10.7 cm solar flux, and southern Oscillation Index (SOI) are publicly available at Amplitudes observed in SAO, AO, QBO (26 months), QBO (30 months), ENSO (60 months), and solar (132 months) over Gadanki Corresponding phases are shown in bottom panels, respectively.

The above figure shows the amplitude (top) and phase (bottom) of the SAO, AO, QBO (26 months), QBO (30 months), ENSO (60 months) periods derived from lidar measurements over Gadanki at each altitude. Note that the SAO, AO, QBO, and ENSO amplitude and phases at each altitude are obtained using the least squares method applied for monthly mean temperatures. The amplitudes of these oscillations are small.
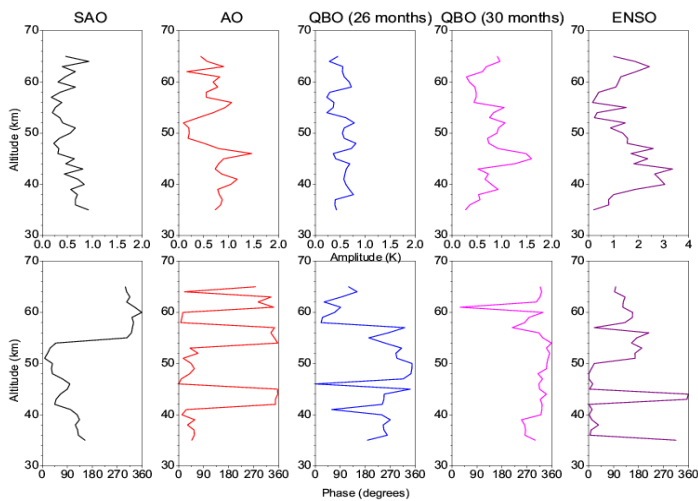
Fig.9: Phase versus Altitude

Using SABER measurements, Huang et al. [2006] reported the temperature amplitudes of SAO contours over 48°S-48°N for the altitudes 15 to 95 km. They observed maximum SAO amplitude observed at 72 km, and minimum at ~82 km for the latitude ~23°S. Compared to the SAO, the observed AO amplitude is higher in both the stratosphere and mesosphere. The phases of the SAO and AO observed by the lidar show a downward progression below 60 km, and above that altitude no clear phase progression is seen. Note that we also obtained amplitude and phases of QBO with 30-month periods. The 26 and 30-month periods of the QBO amplitudes are similar below 60 km. The amplitude peak of about 1.3 K is observed at ~70 km in the 26-month QBO. Details of the solar component along with QBO and ENSO will be discussed in the next sub-section.

2.8 QBO, ENSO and Solar variations in temperature

The below Figure shows the temperature response to the QBO, ENSO and 11-year solar cycle derived from the regression analysis using the time series of lidar as a function of altitude. Also, we found that, above 60 km the QBO response is larger and relatively smaller response is observed in the lower altitude levels. Inter-annual variability of temperature and zonal wind in the tropical stratosphere is strongly influenced by the QBO [Baldwin et al. 2001]. A strong ENSO positive maxima of 1.2 K/SOI at 45 km, and strong a negative maximum of -1 K/SOI was found near 60 km in the Gadanki lidar temperature data sets. The negative maxima of ENSO from the lidar and satellite are in good agreement.

The monthly analysis of these data sets reveals three different types of temperature signatures, following three distinct vertical shapes. In general, significant negative solar flux coefficients, and it turns to positive solar coefficients at above 55 km altitude region. Similar negative solar flux values are observed Sridharan et al. [2009] in the stratosphere region and they noted positive solar coefficient values above 60 km using the same lidar but using the data up to 2007. In some altitudes a positive response can be noted, however the significance is not sufficient in the upper stratosphere. However, a signature of 1 to 2 K appears in the upper stratosphere and lower mesosphere (45 to 65 km). Remsberg and Deaver [2005] observed 11-year solar cycle using the HALOE for the period of 1991 to 2004 and for the upper stratosphere and mesosphere for latitude zones from 40°N to 40°S, they found 11-year solar cycle term of amplitude of about 0.5 to 1.7 K in temperature versus pressure time series.
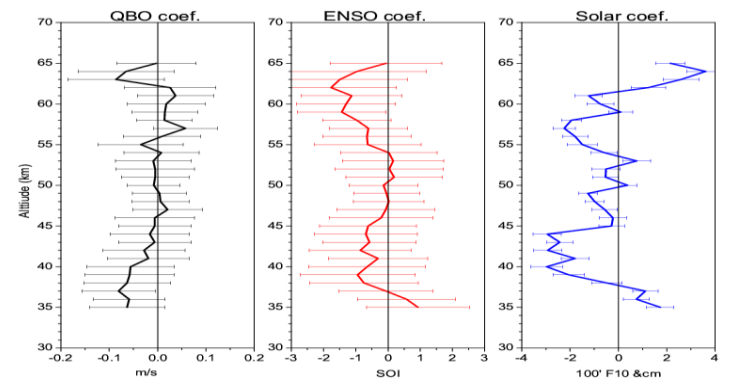

Fig.10: Coefficient observed in QBO, ENSO and Solar with Height

Coefficients observed in the QBO (left panels), ENSO (middle panels) and Solar (right panels) using Gadanki lidar observations during 1998-2010.

The positive response to the solar coefficient in the stratosphere was also observed previously by Keckhut et al. [2005] of about 1-2 K in the tropics and negative, but large values at mid-latitudes using three independent temperature datasets. It is attributed to direct absorption of solar radiation by ozone [McCormack and Hood, 1996; Larkin et al., 2000]. Ramaswamy et al. [2001] calculated the solar flux coefficients using nadir viewing satellite observations from 1979 to 1995, and showed a solar component of the order of 0.5-1.0 K throughout most of the low-latitude (30°N-30°S) stratosphere, with a maximum near 40 km altitude level [Ramaswamy et al.,

2001]. The solar cycle signature in stratospheric temperatures need not be uniform and identical all over the globe and at all altitudes. This has been made clear from the work by Labitzke and van Loon [1997] on the horizontal scale, as well as on the vertical scale in the work by Chanin and Keckhut [1991], and may be attributable to the role of planetary waves.

2.9 Long-term Trends

The altitude profiles of the estimated linear trend coefficients are plotted in the below Figure. This Figure shows the profile of temperature trend observed over Gadanki using lidar measurements along with two sigma error limits. In general, the cooling trends of 0.9 K/decade are estimated near 35 km. This cooling increases with altitude and attain values of 3-3.5 K/decade near 38 km then decreases to 1 K/decade near 48 km. The maximum cooling trend at 38 km is consistent with earlier analysis of SAGE II data, which show the cooling trend peak at 40 km [Newchurch et al., 2000]. Another stronger cooling is observed over Gadanki around 57 km. Recently, Sridharan et al. [2009] observed stronger cooling at 37 km and 57 km using same lidar data but up to the year 2007. The observed maximum cooling trend is relatively low as compared to the earlier analysis of HALOE data [Randel et al., 1999].

In general, there is a uniform cooling trend of about 0.77 K/decade between 40 and 55 km, followed by increasing cooling with altitude. At this location there is good agreement for the magnitudes of the temperature trend responses between the satellite and the lidar observations. A stronger cooling trend is observed at about 38 km altitude level in Gadanki lidar. Using HALOE satellite temperature measurements during 1992-2004, Fadnavis and Beig [2006] observed a stronger cooling trend around 35 km over the tropics (0-30°N) and then decreases near the stratopause. Using series of Rocketsonde and radiosonde data over the equatorial station Beig and Fadnavis [2001] observed a negative trend of 2-3 K/decade in the lower mesosphere and a rise in cooling to 5-6 K/decade at 70 km, the two standard deviation error is found to range from + 0.5 K/decade in the lower mesosphere to ±1.3 K/decade in the middle mesosphere.
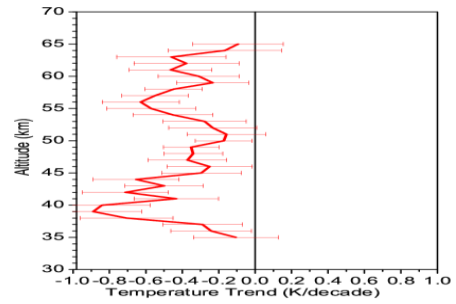

Fig.11: Temperature trend versus Altitude

Long-term trends observed at different altitudes obtained using Gadanki lidar observations during 1998 to 2010. Horizontal bars show the standard deviations.

Table 2: Long-term trends observed using Gadanki lidar along with that those observed from satellite (HALOE+SABER) observations. The values reported in Remsberg [2009] are also provided.

Altitude (Km)	Gadanki (13.5N) 1998-2008 (K/dec)	HALOE + SABER 13.5N +/- 5 1992-2011 (K/dec)	Remsberg_jgr2009 10 +/-5 1991-2005 (K/dec)
40	-2.9 ± 0.27	-1.08 ± 0.13	------------
50	-0.69 ± 0.16	-1.90 ± 0.14	-0.7 ± 0.17
60	-1.24 ± 0.22	-3.52 ± 0.23	-1.2 ± 0.16

Calculated long-term trend amplitudes at different selected altitude levels are shown in **Table 2**.The amplitudes are shown for both Lidar data sets and the combined HALOE and SABER satellite measurements (as depicted in the earlier **Figure 12**). The table summarizes the representative amplitude values for the lower stratosphere (40 km), stratopause (50 km) and lower mesosphere (60 km) altitude regions. In general, the satellite measurements show higher amplitudes than the Lidar observations. However, the results show a high negative value for this location by satellite and the difference are found to be higher between Lidar and satellites. The results are compared with the earlier observations shown by Remsberg [2009] and are found comparatively for the Gadanki Lidar.

3. SUMMARY AND CONCLUSIONS

Using long-term temperature data from the Gadanki Lidar located at a low latitude station; long-term trends observed in the temperatures are reported, including SAO, AO, QBO, ENSO and solar cycle oscillations prevailing in the stratosphere and the lower mesosphere. These oscillations extracted from Lidar are compared with those derived from the satellite (HALOE and

SABER) observations and that are reported in the literature. The main findings are summarized in the following:

Entire data set has been segregated based on the number of hours available in each of the night operation of the Gadanki Lidar data. This segregation is very much useful to investigate several issues, including long-term oscillations, planetary and gravity waves and long-term trends.

The mean thermal structure over low latitude is presented using the long-term data available from Gadanki Lidar observations that is available with minimum of 2 hours of observations in each night (to minimize the errors).

The mean monthly temperatures show clear semiannual oscillations around 40-50 km, corresponding to the stratopause semiannual oscillation (SSAO), and 70-80 km, corresponding to the mesospheric semiannual oscillation (MSAO).

The frequency distribution of stratopause altitude and the temperature show that the peak stratopause altitude is around 46-48 km and temperature is in the range of 265-268 K. Both the stratopause altitude and temperature show clear semiannual oscillation.

Strong semiannual variation in the occurrence of MTIs with peak during equinoctial months is noticed. Although the peak occurrence is seen during March and October, broad maximum from March-May and September-November is noticed.

The amplitudes of MTIs are stronger during May-June and November with sharp changes in April-May and October-November months.

The starting and ending altitudes of MTIs also show maxima during the equinoxes.

Amplitudes and the phases of all the long-period oscillations are extracted and removed to investigate the long-term trends. The amplitudes of these oscillations are found to be from 0.5 K to 2 K.

A strong ENSO positive maxima of 1.2 K/SOI at 45 km, and strong a negative maximum of -1 K/SOI was found near 60 km in the Gadanki lidar temperature data sets.

In general, the cooling trends of 0.9 K/decade is noticed near 35 km. This cooling increases with altitude and attain values of 3-3.5 K/decade near 38 km then decreases to 1 K/decade near 48 km.

REFERENCES

1. Andrews DG, Holton JR, Leovy CB. Middle Atmosphere Dynamics, 489 pp. Orlando, FL: Academic Press; 1987.[Google Scholar]

2. Baldwin MP, O&apos D, Sullivan. Stratospheric effects of ENSO-related tropospheric circulation anomalies. J. Clim 1994; 8(4):649-66. [Google Scholar]

3. Barnett JJ, Corney M. Middle Atmosphere Reference Model from Satellite Data. Middle Atmosphere Program, MAP Handbook 1985; 16:47-85. [Google Scholar]

4. Beig G, Fadnavis S. 2001), In Search of Greenhouse Signals in the Equatorial Middle Atmosphere. In Search of Greenhouse Signals in the Equatorial Middle Atmosphere, Geophys. Res. Lett 2001; 28(24):4603-4606. [Google Scholar]

5. Beig G. Review of mesospheric temperature trends, Rev. Geophys 2003; 41(4):10-1029. [Google Scholar]

6. Burrage MD, Vincent RA, Mayr HG, Skinner WR, Arnold NF, Hays PB. Long-term variability of the equatorial middle atmosphere zonal wind. J. Geophys. Res 1996; 101:12-847. [Google Scholar]

7. Canziani PO, Holton JR, Fishbein E, Frodievaux L, Waters JW. Equatorial Kelvin Waves: A. Equatorial Kelvin Waves: A UARS MLS View, J. Atmos. Sci 1994; 51:3053-3076. [Google Scholar]

8. Chakravarty SC, Datta J, Revankar CP. Climatology of long-period oscillations in the equatorial middle atmosphere over. Thumba, Curr. Sci 1992;63:33-42. [Google Scholar]

9. Nee JB, Thulasiraman S, Chen WN, M Venkat Ratnam, , Narayana D. Rao (2002), Middle atmospheric temperature structure over two tropical locations, Chung Li (25°N, 121°E) and Gadanki. ; 64:1311-1319. [Google Scholar]

10. Ramaswamy V. Stratospheric temperature trends: Observations and model simulations. and quot. Reviews of Geophysics 2001; 39(1):71-122. [Google Scholar]